16. N. P. Ong, *Phys. Rev. B* **43**, 193 (1991).
17. P. L. Taylor, *Proc. R. Soc. Lond. A Math. Phys. Sci.* **275**, 209 (1963).
18. J. W. Orenstein *et al.*, *Phys. Rev. B* **42**, 6342 (1990).
19. Z. Schlesinger *et al.*, *Phys. Rev. B* **41**, 11237 (1990).
20. H. L. Liu *et al.*, *J. Phys. Condens. Matter* **11**, 239 (1999).
21. D. van der Marel *et al.*, *Nature* **425**, 271 (2003).
22. C. C. Homes *et al.*, *Nature* **430**, 539 (2004).
23. T. Valla *et al.*, *Science* **285**, 2110 (1999).
24. S. Kasahara *et al.*, *Phys. Rev. B* **81**, 184519 (2010).
25. H. Shishido *et al.*, *Phys. Rev. Lett.* **104**, 057008 (2010).
26. N. Doiron-Leyraud *et al.*, *Eur. Phys. J. B* **78**, 23 (2010).
27. J. S. Brooks, *Rep. Prog. Phys.* **71**, 126501 (2008).
28. M. A. Tanatar, J. Paglione, C. Petrovic, L. Taillefer, *Science* **316**, 1320 (2007).
29. R. Settai *et al.*, *J. Phys. Condens. Matter* **13**, L627 (2001).
30. A. McCollam, S. R. Julian, P. M. C. Rourke, D. Aoki, J. Flouquet, *Phys. Rev. Lett.* **94**, 186401 (2005).
31. J. S. Kim, D. Hall, K. Heuser, G. R. Stewart, *Solid State Commun.* **114**, 413 (2000).
32. N. Kimura *et al.*, *Physica B* **281-282**, 710 (2000).
33. R. Daou, C. Bergemann, S. R. Julian, *Phys. Rev. Lett.* **96**, 026401 (2006).
34. M. Takashita *et al.*, *J. Phys. Soc. Jpn.* **65**, 515 (1996).
35. R. Hlubina, T. M. Rice, *Phys. Rev. B* **51**, 9253 (1995).
36. A. Rosch, *Phys. Rev. Lett.* **82**, 4280 (1999).
37. J. M. Ziman, *Electrons and Phonons* (Clarendon Press, Oxford, UK, 1960).
38. S. S. Adler *et al.*; PHENIX Collaboration, *Phys. Rev. Lett.* **91**, 182301 (2003).
39. T. Schäfer, *Phys. Rev. A* **76**, 063618 (2007).
40. C. Cao *et al.*, *Science* **331**, 58 (2011).
41. D. A. Teaney, *arXiv*:0905.2433v1.
42. P. K. Kovtun, D. T. Son, A. O. Starinets, *Phys. Rev. Lett.* **94**, 111601 (2005).
43. A. V. Andreev, S. A. Kivelson, B. Spivak, *Phys. Rev. Lett.* **106**, 256804 (2011).
44. A. Kaminski *et al.*, *Phys. Rev. B* **71**, 014517 (2005).

Acknowledgments: We are pleased to acknowledge the help of M. Baenitz, M. Nicklas, and C. Klausnitzer of the Max Planck Institute for the Chemical Physics of Solids in Dresden, where the high-temperature resistivity measurements on $Sr_3Ru_2O_7$ were performed, and useful discussions with J. Orenstein, S. A. Kivelson, C. A. Hooley, and J. Zaanen. The research was supported by the UK Engineering and Physical Sciences Research Council. H.S. gratefully acknowledges fellowships from the Canon Foundation Europe and Marubun Research Promotion Foundation, and A.P.M. acknowledges the receipt of a Royal Society–Wolfson Merit Award.

Supplementary Materials

www.sciencemag.org/cgi/content/full/339/6121/804/DC1
Materials and Methods
Supplementary Text
Fig. S1
Tables S1 to S10
References (*45*–*65*)

18 July 2012; accepted 27 November 2012
10.1126/science.1227612

Detection of the Characteristic Pion-Decay Signature in Supernova Remnants

M. Ackermann,[1] M. Ajello,[2] A. Allafort,[3] L. Baldini,[4] J. Ballet,[5] G. Barbiellini,[6,7] M. G. Baring,[8] D. Bastieri,[9,10] K. Bechtol,[3] R. Bellazzini,[11] R. D. Blandford,[3] E. D. Bloom,[3] E. Bonamente,[12,13] A. W. Borgland,[3] E. Bottacini,[3] T. J. Brandt,[14] J. Bregeon,[11] M. Brigida,[15,16] P. Bruel,[17] R. Buehler,[3] G. Busetto,[9,10] S. Buson,[9,10] G. A. Caliandro,[18] R. A. Cameron,[3] P. A. Caraveo,[19] J. M. Casandjian,[5] C. Cecchi,[12,13] Ö. Çelik,[14,20,21] E. Charles,[3] S. Chaty,[5] R. C. G. Chaves,[5] A. Chekhtman,[22] C. C. Cheung,[23] J. Chiang,[3] G. Chiaro,[24] A. N. Cillis,[14,25] S. Ciprini,[13,26] R. Claus,[3] J. Cohen-Tanugi,[27] L. R. Cominsky,[28] J. Conrad,[29,30,31] S. Corbel,[5,32] S. Cutini,[33] F. D'Ammando,[12,34,35] A. de Angelis,[36] F. de Palma,[15,16] C. D. Dermer,[37] E. do Couto e Silva,[3] P. S. Drell,[3] A. Drlica-Wagner,[3] L. Falletti,[27] C. Favuzzi,[15,16] E. C. Ferrara,[14] A. Franckowiak,[3] Y. Fukazawa,[38] S. Funk,[3]* P. Fusco,[15,16] F. Gargano,[16] S. Germani,[12,13] N. Giglietto,[15,16] P. Giommi,[33] F. Giordano,[15,16] M. Giroletti,[39] T. Glanzman,[3] G. Godfrey,[3] I. A. Grenier,[5] M.-H. Grondin,[40,41] J. E. Grove,[37] S. Guiriec,[14] D. Hadasch,[18] Y. Hanabata,[38] A. K. Harding,[14] M. Hayashida,[3,42] K. Hayashi,[38] E. Hays,[14] J. W. Hewitt,[14] A. B. Hill,[3,43] R. E. Hughes,[44] M. S. Jackson,[30,45] T. Jogler,[3] G. Jóhannesson,[46] A. S. Johnson,[3] T. Kamae,[3] J. Kataoka,[47] J. Katsuta,[3] J. Knödlseder,[48,49] M. Kuss,[11] J. Lande,[3] S. Larsson,[29,30,50] L. Latronico,[51] M. Lemoine-Goumard,[52,53] F. Longo,[6,7] F. Loparco,[15,16] M. N. Lovellette,[37] P. Lubrano,[12,13] G. M. Madejski,[3] F. Massaro,[3] M. Mayer,[1] M. N. Mazziotta,[16] J. E. McEnery,[14,54] J. Mehault,[27] P. F. Michelson,[3] R. P. Mignani,[55] W. Mitthumsiri,[3] T. Mizuno,[56] A. A. Moiseev,[20,54] M. E. Monzani,[3] A. Morselli,[57] I. V. Moskalenko,[3] S. Murgia,[3] T. Nakamori,[47] R. Nemmen,[14] E. Nuss,[27] M. Ohno,[58] T. Ohsugi,[56] N. Omodei,[3] M. Orienti,[39] E. Orlando,[3] J. F. Ormes,[59] D. Paneque,[3,60] J. S. Perkins,[14,21,20,61] M. Pesce-Rollins,[11] F. Piron,[27] G. Pivato,[10] S. Rainò,[15,16] R. Rando,[9,10] M. Razzano,[11,62] S. Razzaque,[22] A. Reimer,[3,63] O. Reimer,[3,63] S. Ritz,[62] C. Romoli,[10] M. Sánchez-Conde,[3] A. Schulz,[1] C. Sgrò,[11] P. E. Simeon,[3] E. J. Siskind,[64] D. A. Smith,[52] G. Spandre,[11] P. Spinelli,[15,16] F. W. Stecker,[14,65] A. W. Strong,[66] D. J. Suson,[67] H. Tajima,[3,68] H. Takahashi,[38] T. Takahashi,[58] T. Tanaka,[3,69]* J. G. Thayer,[3] J. B. Thayer,[3] D. J. Thompson,[14] S. E. Thorsett,[70] L. Tibaldo,[9,10] O. Tibolla,[71] M. Tinivella,[11] E. Troja,[14,72] Y. Uchiyama,[3]* T. L. Usher,[3] J. Vandenbroucke,[3] V. Vasileiou,[27] G. Vianello,[3,73] V. Vitale,[57,74] A. P. Waite,[3] M. Werner,[63] B. L. Winer,[44] K. S. Wood,[37] M. Wood,[3] R. Yamazaki,[75] Z. Yang,[29,30] S. Zimmer[29,30]

Cosmic rays are particles (mostly protons) accelerated to relativistic speeds. Despite wide agreement that supernova remnants (SNRs) are the sources of galactic cosmic rays, unequivocal evidence for the acceleration of protons in these objects is still lacking. When accelerated protons encounter interstellar material, they produce neutral pions, which in turn decay into gamma rays. This offers a compelling way to detect the acceleration sites of protons. The identification of pion-decay gamma rays has been difficult because high-energy electrons also produce gamma rays via bremsstrahlung and inverse Compton scattering. We detected the characteristic pion-decay feature in the gamma-ray spectra of two SNRs, IC 443 and W44, with the Fermi Large Area Telescope. This detection provides direct evidence that cosmic-ray protons are accelerated in SNRs.

A supernova explosion drives its progenitor material supersonically into interstellar space, forming a collisionless shock wave ahead of the stellar ejecta. The huge amount of kinetic energy released by a supernova, typically 10^{51} ergs, is initially carried by the expanding ejecta and is then transferred to kinetic and thermal energies of shocked interstellar gas and relativistic particles. The shocked gas and relativistic particles produce the thermal and nonthermal emissions of a supernova remnant (SNR). The mechanism of diffusive shock acceleration (DSA) can explain the production of relativistic particles in SNRs (*1*). DSA generally predicts that a substantial fraction of the shock energy is transferred to relativistic protons. Indeed, if SNRs are the main sites of acceleration of the galactic cosmic rays, then 3 to 30% of the supernova kinetic energy must end up transferred to relativistic protons. However, the presence of relativistic protons in SNRs has been mostly inferred from indirect arguments (*2*–*5*).

A direct signature of high-energy protons is provided by gamma rays generated in the decay of neutral pions (π^0); proton-proton (more generally nuclear-nuclear) collisions create π^0 mesons, which usually quickly decay into two gamma rays (*6*–*8*) (schematically written as $p + p \rightarrow \pi^0 +$ other products, followed by $\pi^0 \rightarrow 2\gamma$), each having an energy of $m_{\pi^0}c^2/2 = 67.5$ MeV in the rest frame of the neutral pion (where m_{π^0} is the rest mass of the neutral pion and c is the speed of light). The gamma-ray number spectrum, $F(\varepsilon)$, is thus symmetric about 67.5 MeV in a log-log representation (*9*). The π^0-decay spectrum in the usual $\varepsilon^2 F(\varepsilon)$ representation rises steeply below ~200 MeV and approximately traces the energy distribution of parent protons at energies greater than a few GeV. This characteristic spectral feature (often referred to as the "pion-decay bump") uniquely identifies π^0-decay gamma rays and thereby high-energy protons, allowing a measurement of the source spectrum of cosmic rays.

Massive stars are short-lived and end their lives with core-collapse supernova explosions. These explosions typically occur in the vicinity of molecular clouds with which they interact. When cosmic-ray protons accelerated by SNRs penetrate into high-density clouds, π^0-decay gamma-ray emission is expected to be enhanced because of more frequent *pp* interactions relative to the interstellar medium (*10*). Indeed, SNRs

interacting with molecular clouds are the most luminous SNRs in gamma rays (*11*, *12*). The best examples of SNR-cloud interactions in our galaxy are the SNRs IC 443 and W44 (*13*), which are the two highest-significance SNRs in the second Fermi Large Area Telescope (LAT) catalog (2FGL) (*14*) and are thus particularly suited for a dedicated study of the details of their gamma-ray spectra. The age of each remnant is estimated to be ~10,000 years. IC 443 and W44 are located at distances of 1.5 kpc and 2.9 kpc, respectively.

We report here on 4 years of observations with the Fermi LAT (4 August 2008 to 16 July 2012) of IC 443 and W44, focusing on the sub-GeV part of the gamma-ray spectrum—a crucial spectral window for distinguishing π^0-decay gamma rays from electron bremsstrahlung or inverse Compton scattering produced by relativistic electrons. Previous analyses of IC 443 and W44 used only 1 year of Fermi LAT data (*15*–*17*) and were limited to the energy band above 200 MeV, mainly because of the small and rapidly changing LAT effective area at low energies. A recent update to the event classification and background rejection (so-called Pass 7) provides an increase in LAT effective area at 100 MeV by a factor of ~5 (*18*), enabling the study of bright, steady sources in the galactic plane below 200 MeV with the Fermi LAT. Note that the gamma-ray spectral energy distribution of W44 measured recently by the AGILE satellite falls steeply below 1 GeV, which the authors interpreted as a clear indication for the π^0-decay origin of the gamma-ray emission (*19*). Also, a recent analysis of W44 at high energies (above 2 GeV) has been reported (*20*), revealing large-scale gamma-ray emission attributable to high-energy protons that have escaped from W44. Here, we present analyses of the gamma-ray emission from the compact regions delineated by the radio continuum emission of IC 443 and W44.

The analysis was performed using the Fermi LAT Science Tools (*21*). We used a maximum likelihood technique to determine the significance of a source over the background and to fit spectral parameters (*22*, *23*). For both SNRs, additional sources seen as excesses in the background-subtracted map have been added to the background model (*24*) and are shown as diamonds in Fig. 1—one in the case of IC 443, three in the case of W44. The inclusion of these sources had no influence on the fitted spectrum of the SNRs. Three close-by sources (2FGL J1852.8+0156c, 2FGL J1857.2+0055c, and 2FGL J1858.5+0129c) have been identified with escaping cosmic rays from W44 (*20*). These 2FGL sources have been removed from the background model (see below) in order to measure the full cosmic-ray content of W44.

Figure 2 shows the spectral energy distribution obtained for IC 443 and W44 through maximum likelihood estimation. To derive the flux points, we performed a maximum likelihood fitting in 24 independent logarithmically spaced energy bands from 60 MeV to 100 GeV. The normalization of the fluxes of IC 443 and W44, and those of neighboring sources and of the galactic diffuse model, was left free in the fit for each bin. In both sources, the spectra below ~200 MeV are steeply rising, clearly exhibiting a break at ~200 MeV. To quantify the significances of the spectral breaks, we fit the fluxes of IC 443 and W44 between 60 MeV and 2 GeV—below the high-energy breaks previously found in the 1-year spectra (*15*, *16*)—with both a single power law of the form $F(\varepsilon) = K(\varepsilon/\varepsilon_0)^{-\Gamma_1}$ and a smoothly broken power law of the form $F(\varepsilon) = K(\varepsilon/\varepsilon_0)^{-\Gamma_1}[1 + (\varepsilon/\varepsilon_{br})^{(\Gamma_2-\Gamma_1)/\alpha}]^{-\alpha}$ with $\varepsilon_0 = 200$ MeV. The spectral index changes from Γ_1 to Γ_2 ($>\Gamma_1$) at the break energy ε_{br}. The smoothness of the break is determined by the parameter α, which was fixed at 0.1 (Table 1). We define the test-statistic value (*TS*) as $2\ln(\mathcal{L}_1/\mathcal{L}_0)$, where $\mathcal{L}_{1/0}$ corresponds to the likelihood value for the source/no-source hypothesis (*24*). The detection significance is given by $\sim\sqrt{TS}$. The smoothly broken power law model yields a significantly larger *TS* than a single power law, establishing the existence of a low-energy break. The improvement in log likelihood when comparing the broken power law to a single power law corresponds to a formal statistical significance of 19σ for the

[1]Deutsches Elektronen Synchrotron (DESY), D-15738 Zeuthen, Germany. [2]Space Sciences Laboratory, University of California, Berkeley, CA 94720, USA. [3]W. W. Hansen Experimental Physics Laboratory, Kavli Institute for Particle Astrophysics and Cosmology, Department of Physics, and SLAC National Accelerator Laboratory, Stanford University, Stanford, CA 94305, USA. [4]Università di Pisa and Istituto Nazionale di Fisica Nucleare, Sezione di Pisa, I-56127 Pisa, Italy. [5]Laboratoire AIM, CEA-IRFU/CNRS/Université Paris Diderot, Service d'Astrophysique, CEA Saclay, 91191 Gif-sur-Yvette, France. [6]Istituto Nazionale di Fisica Nucleare, Sezione di Trieste, I-34127 Trieste, Italy. [7]Dipartimento di Fisica, Università di Trieste, I-34127 Trieste, Italy. [8]Rice University, Department of Physics and Astronomy, MS-108, Post Office Box 1892, Houston, TX 77251, USA. [9]Istituto Nazionale di Fisica Nucleare, Sezione di Padova, I-35131 Padova, Italy. [10]Dipartimento di Fisica e Astronomia "G. Galilei," Università di Padova, I-35131 Padova, Italy. [11]Istituto Nazionale di Fisica Nucleare, Sezione di Pisa, I-56127 Pisa, Italy. [12]Istituto Nazionale di Fisica Nucleare, Sezione di Perugia, I-06123 Perugia, Italy. [13]Dipartimento di Fisica, Università degli Studi di Perugia, I-06123 Perugia, Italy. [14]NASA Goddard Space Flight Center, Greenbelt, MD 20771, USA. [15]Dipartimento di Fisica "M. Merlin" dell'Università e del Politecnico di Bari, I-70126 Bari, Italy. [16]Istituto Nazionale di Fisica Nucleare, Sezione di Bari, 70126 Bari, Italy. [17]Laboratoire Leprince-Ringuet, École Polytechnique, CNRS/IN2P3, 91128 Palaiseau, France. [18]Institut de Ciències de l'Espai (IEEE-CSIC), Campus UAB, 08193 Barcelona, Spain. [19]INAF–Istituto di Astrofisica Spaziale e Fisica Cosmica, I-20133 Milano, Italy. [20]Center for Research and Exploration in Space Science and Technology (CRESST) and NASA Goddard Space Flight Center, Greenbelt, MD 20771, USA. [21]Department of Physics and Center for Space Sciences and Technology, University of Maryland Baltimore County, Baltimore, MD 21250, USA. [22]Center for Earth Observing and Space Research, College of Science, George Mason University, Fairfax, VA 22030, resident at Naval Research Laboratory, Washington, DC 20375, USA. [23]National Research Council Research Associate, National Academy of Sciences, Washington, DC 20001, resident at Naval Research Laboratory, Washington, DC 20375, USA. [24]INFN and Dipartimento di Fisica e Astronomia "G. Galilei," Università di Padova, I-35131 Padova, Italy. [25]Instituto de Astronomía y Fisica del Espacio, Parbellón IAFE, Cdad. Universitaria, C1428ZAA Buenos Aires, Argentina. [26]ASI Science Data Center, I-00044 Frascati (Roma), Italy. [27]Laboratoire Univers et Particules de Montpellier, Université Montpellier 2, CNRS/IN2P3, Montpellier, France. [28]Department of Physics and Astronomy, Sonoma State University, Rohnert Park, CA 94928, USA. [29]Department of Physics, Stockholm University, AlbaNova, SE-106 91 Stockholm, Sweden. [30]Oskar Klein Centre for Cosmoparticle Physics, AlbaNova, SE-106 91 Stockholm, Sweden. [31]Royal Swedish Academy of Sciences Research Fellow, funded by a grant from the K. A. Wallenberg Foundation. [32]Institut Universitaire de France, 75005 Paris, France. [33]Agenzia Spaziale Italiana (ASI) Science Data Center, I-00044 Frascati (Roma), Italy. [34]IASF Palermo, 90146 Palermo, Italy. [35]INAF–Istituto di Astrofisica Spaziale e Fisica Cosmica, I-00133 Roma, Italy. [36]Dipartimento di Fisica, Università di Udine and Istituto Nazionale di Fisica Nucleare, Sezione di Trieste, Gruppo Collegato di Udine, I-33100 Udine, Italy. [37]Space Science Division, Naval Research Laboratory, Washington, DC 20375, USA. [38]Department of Physical Sciences, Hiroshima University, Higashi-Hiroshima, Hiroshima 739-8526, Japan. [39]INAF Istituto di Radioastronomia, 40129 Bologna, Italy. [40]Max-Planck-Institut für Kernphysik, D-69029 Heidelberg, Germany. [41]Landessternwarte, Universität Heidelberg, Königstuhl, D-69117 Heidelberg, Germany. [42]Department of Astronomy, Graduate School of Science, Kyoto University, Sakyo-ku, Kyoto 606-8502, Japan. [43]School of Physics and Astronomy, University of Southampton, Highfield, Southampton SO17 1BJ, UK. [44]Department of Physics, Center for Cosmology and Astro-Particle Physics, Ohio State University, Columbus, OH 43210, USA. [45]Department of Physics, Royal Institute of Technology (KTH), AlbaNova, SE-106 91 Stockholm, Sweden. [46]Science Institute, University of Iceland, IS-107 Reykjavik, Iceland. [47]Research Institute for Science and Engineering, Waseda University, 3-4-1, Okubo, Shinjuku, Tokyo 169-8555, Japan. [48]CNRS, IRAP, F-31028 Toulouse Cedex 4, France. [49]GAHEC, Université de Toulouse, UPS-OMP, IRAP, 31028 Toulouse, France. [50]Department of Astronomy, Stockholm University, SE-106 91 Stockholm, Sweden. [51]Istituto Nazionale di Fisica Nucleare, Sezione di Torino, I-10125 Torino, Italy. [52]Université Bordeaux 1, CNRS/IN2p3, Centre d'Études Nucléaires de Bordeaux Gradignan, 33175 Gradignan, France. [53]Funded by contract ERC-StG-259391 from the European Community. [54]Department of Physics and Department of Astronomy, University of Maryland, College Park, MD 20742, USA. [55]Mullard Space Science Laboratory, University College London, Holmbury St. Mary, Dorking, Surrey RH5 6NT, UK. [56]Hiroshima Astrophysical Science Center, Hiroshima University, Higashi-Hiroshima, Hiroshima 739-8526, Japan. [57]Istituto Nazionale di Fisica Nucleare, Sezione di Roma "Tor Vergata," I-00133 Roma, Italy. [58]Institute of Space and Astronautical Science, JAXA, 3-1-1 Yoshinodai, Chuo-ku, Sagamihara, Kanagawa 252-5210, Japan. [59]Department of Physics and Astronomy, University of Denver, Denver, CO 80208, USA. [60]Max-Planck-Institut für Physik, D-80805 München, Germany. [61]Harvard-Smithsonian Center for Astrophysics, Cambridge, MA 02138, USA. [62]Santa Cruz Institute for Particle Physics, Department of Physics, and Department of Astronomy and Astrophysics, University of California, Santa Cruz, CA 95064, USA. [63]Institut für Astro- und Teilchenphysik and Institut für Theoretische Physik, Leopold-Franzens-Universität Innsbruck, A-6020 Innsbruck, Austria. [64]NYCB Real-Time Computing Inc., Lattingtown, NY 11560, USA. [65]Department of Physics and Astronomy, University of California, Los Angeles, CA 90095, USA. [66]Max-Planck-Institut für Extraterrestrische Physik, 85748 Garching, Germany. [67]Department of Chemistry and Physics, Purdue University Calumet, Hammond, IN 46323, USA. [68]Solar-Terrestrial Environment Laboratory, Nagoya University, Nagoya 464-8601, Japan. [69]Department of Physics, Graduate School of Science, Kyoto University, Sakyo-ku, Kyoto 606-8502, Japan. [70]Department of Physics, Willamette University, Salem, OR 97031, USA. [71]Institut für Theoretische Physik und Astrophysik, Universität Würzburg, D-97074 Würzburg, Germany. [72]NASA Postdoctoral Program Fellow. [73]Consorzio Interuniversitario per la Fisica Spaziale, I-10133 Torino, Italy. [74]Dipartimento di Fisica, Università di Roma "Tor Vergata," I-00133 Roma, Italy. [75]Department of Physics and Mathematics, Aoyama Gakuin University, Sagamihara, Kanagawa 252-5258, Japan.

*To whom correspondence should be addressed. E-mail: funk@slac.stanford.edu (S.F.); ttanaka@cr.scphys.kyoto-u.ac.jp (T.T.); uchiyama@slac.stanford.edu (Y.U.)

low-energy break in IC 443 and 21σ for that in W44, when assuming a nested model with two additional degrees of freedom.

To determine whether the spectral shape could indeed be modeled with accelerated protons, we fit the LAT spectral points with a π^0-decay spectral model, which was numerically calculated from a parameterized energy distribution of relativistic protons. Following previous studies (*15*, *16*), the parent proton spectrum as a function of momentum p was parameterized by a smoothly broken power law in the form of

$$\frac{dN_p}{dp} \propto p^{-s_1}\left[1+\left(\frac{p}{p_{\rm br}}\right)^{\frac{s_2-s_1}{\beta}}\right]^{-\beta} \quad (1)$$

Best-fit parameters were searched using χ^2-fitting to the flux points. The measured gamma-ray spectra, in particular the low-energy parts, matched the π^0-decay model (Fig. 2). Parameters for the underlying proton spectrum are $s_1 = 2.36 \pm 0.02$, $s_2 = 3.1 \pm 0.1$, and $p_{\rm br} = 239 \pm 74$ GeV c^{-1} for IC 443, and $s_1 = 2.36 \pm 0.05$, $s_2 = 3.5 \pm 0.3$, and $p_{\rm br} = 22$ GeV c^{-1} for W44 (statistical errors only). In Fig. 3 we show the energy distributions of the high-energy protons derived from the gamma-ray fits. The break $p_{\rm br}$ is at higher energies and is unrelated to the low-energy pion-decay bump seen in the gamma-ray spectrum. If the interaction between a cosmic-ray precursor (i.e., cosmic rays distributed in the shock upstream on scales smaller than ~0.1R, where R is the SNR radius) and adjacent molecular clouds were responsible for the bulk of the observed GeV gamma rays, one would expect a much harder energy spectrum at low energies (i.e., a smaller value for the index s_1), contrary to the Fermi observations. Presumably, cosmic rays in the shock downstream produce the observed gamma rays; the first index s_1 represents the shock acceleration index with possible effects due to energy-dependent propagation, and $p_{\rm br}$ may indicate the momentum above which protons cannot be effectively confined within the SNR shell. Note that $p_{\rm br}$ results in the high-energy break in the gamma-ray spectra at ~20 GeV and ~2 GeV for IC 443 and W44, respectively.

The π^0-decay gamma rays are likely emitted through interactions between "crushed cloud" gas and relativistic protons, both of which are highly compressed by radiative shocks driven into molecular clouds that are overtaken by the blast wave of the SNR (*25*). Filamentary structures of synchrotron radiation seen in a high-resolution radio continuum map of W44 (*26*) support this picture. High-energy particles in the "crushed cloud" can be explained by reacceleration of the preexisting galactic cosmic rays (*25*) and/or freshly accelerated particles that have entered the dense region (*20*). The mass of the shocked gas

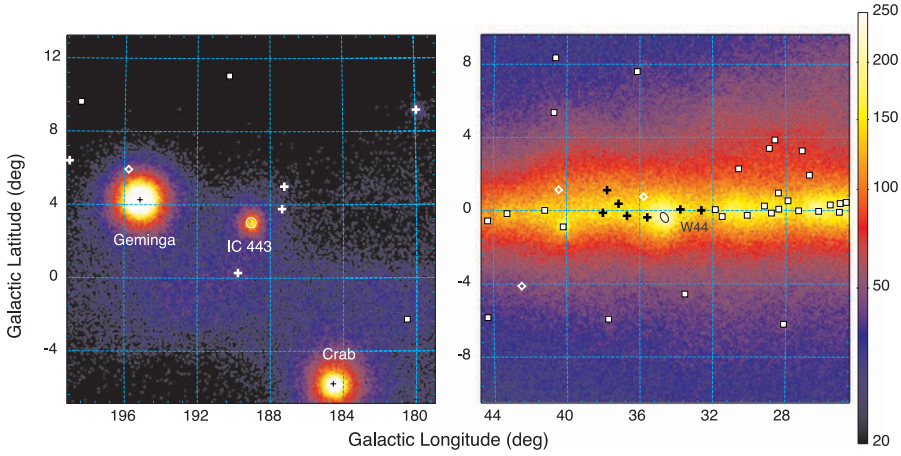

Fig. 1. Gamma-ray count maps of the 20° × 20° fields around IC 443 (**left**) and W44 (**right**) in the energy range 60 MeV to 2 GeV. Nearby gamma-ray sources are marked as crosses and squares. Diamonds denote previously undetected sources. For sources indicated by crosses and diamonds, the fluxes were left as free parameters in the analysis. Events were spatially binned in regions of side length 0.1°, the color scale units represent the square root of count density, and the colors have been clipped at 20 counts per pixel to make the galactic diffuse emission less prominent. Given the spectra of the sources and the effective area of the LAT instrument, the bulk of the photons seen in this plot have energies between 300 and 500 MeV. IC 443 is located in the galactic anti-center region, where the background gamma-ray emission produced by the pool of galactic cosmic rays interacting with interstellar gas is rather weak relative to the region around W44. The two dominant sources in the IC 443 field are the Geminga pulsar (2FGL J0633.9+1746) and the Crab (2FGL J0534.5+2201). For the W44 count map, W44 is the dominant source (subdominant, however, to the galactic diffuse emission).

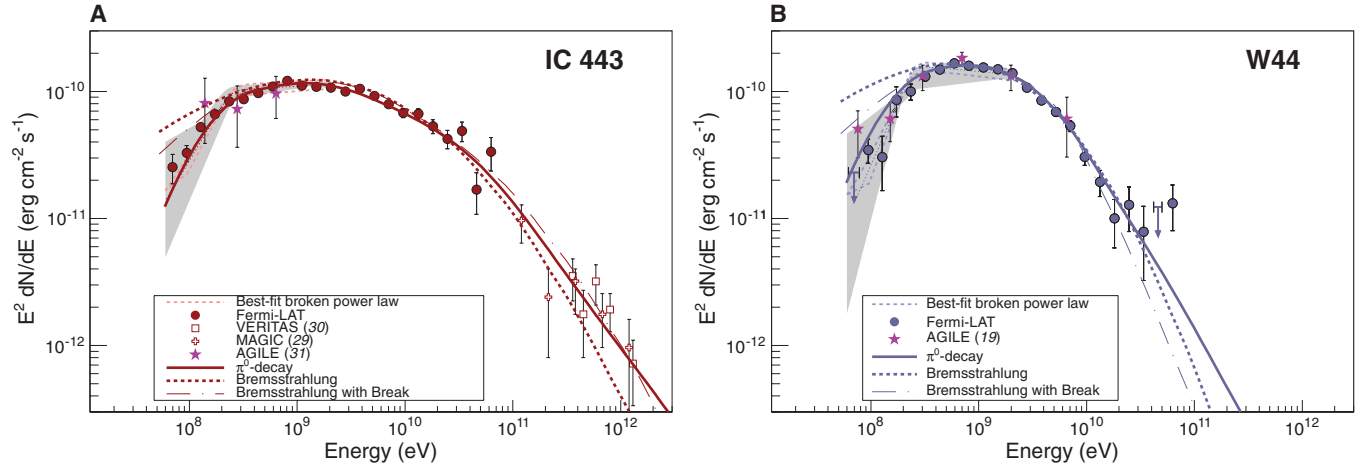

Fig. 2. (**A** and **B**) Gamma-ray spectra of IC 443 (A) and W44 (B) as measured with the Fermi LAT. Color-shaded areas bound by dashed lines denote the best-fit broadband smooth broken power law (60 MeV to 2 GeV); gray-shaded bands show systematic errors below 2 GeV due mainly to imperfect modeling of the galactic diffuse emission. At the high-energy end, TeV spectral data points for IC 443 from MAGIC (*29*) and VERITAS (*30*) are shown. Solid lines denote the best-fit pion-decay gamma-ray spectra, dashed lines denote the best-fit bremsstrahlung spectra, and dash-dotted lines denote the best-fit bremsstrahlung spectra when including an ad hoc low-energy break at 300 MeV c^{-1} in the electron spectrum. These fits were done to the Fermi LAT data alone (not taking the TeV data points into account). Magenta stars denote measurements from the AGILE satellite for these two SNRs, taken from (*31*) and (*19*), respectively.

(~1 × 10^3 $M_\odot$ and ~5 × 10^3 $M_\odot$ for IC 443 and W44, respectively, where $M_\odot$ is the mass of the Sun) is large enough to explain the observed gamma-ray luminosity. Because the "crushed cloud" is geometrically thin, multi-GeV particles are prone to escape from the dense gas, which may explain the break p_{br}.

Escaped cosmic rays reaching the unshocked molecular clouds ahead of the SNR shock can also produce π^0-decay gamma rays (*27*, *28*). Indeed, the gamma rays emitted by the escaped cosmic rays in the large molecular complex that surrounds W44 (total extent of 100 pc) have been identified with three close-by sources (*20*), which led us to remove them from the model in the maximum likelihood analysis, as mentioned above. With this treatment, the measured fluxes below 1 GeV contain small contributions from the escaped cosmic rays, but this does not affect our conclusions. The escaped cosmic rays may significantly contribute to the measured TeV fluxes from IC 443 (*29*, *30*). Emission models could be more complicated. For example, the cosmic-ray precursor with a scale of ~0.1R at the highest energy could interact with the adjacent unshocked molecular gas, producing hard gamma-ray emission. This effect is expected to become important above the LAT energy range.

We should emphasize that radiation by relativistic electrons cannot account for the gamma-ray spectra of the SNRs as naturally as radiation by relativistic protons can (*23*). An inverse-Compton origin of the emission was not plausible on energetic grounds (*11*). The most important seed photon population for scattering is the infrared radiation produced locally by the SNR itself, with an energy density of ~1 eV cm^{-3}, but this is not large enough to explain the observed gamma-ray emission. Unless we introduce in an ad hoc way an additional abrupt break in the electron spectrum at 300 MeV c^{-1} (Fig. 2, dash-dotted lines), the bremsstrahlung models do not fit the observed gamma-ray spectra. If we assume that the same electrons are responsible for the observed synchrotron radiation in the radio band, a low-energy break is not expected to be very strong in the radio spectrum, and thus the existing data do not rule out this scenario. The introduction of the low-energy break introduces additional complexity, and therefore a bremsstrahlung origin is not preferred. Although most of the gamma-ray emission from these SNRs is due to π^0 decay, electron bremsstrahlung may still contribute at a lower level. The Fermi LAT data allow an electron-to-proton ratio K_{ep} of ~0.01 or less, where K_{ep} is defined as the ratio of dN_e/dp and dN_p/dp at p = 1 GeV c^{-1} (figs. S2 and S3).

Finding evidence for the acceleration of protons has long been a key issue in attempts to elucidate the origin of cosmic rays. Our spectral measurements down to 60 MeV enable identification of the π^0-decay feature, thus providing direct evidence for the acceleration of protons in SNRs. The proton momentum distributions, well constrained by the observed gamma-ray spectra, are yet to be understood in terms of acceleration and escape processes of high-energy particles.

Table 1. Spectral parameters in the energy range of 60 MeV to 2 GeV for power-law (PL) and broken power-law (BPL) models. TS = 2 ln($\mathcal{L}_1/\mathcal{L}_0$) is the test-statistic value.

Model	K (cm^2 s^{-1} MeV^{-1})	Γ_1	Γ_2	ε_{br} (MeV)	TS
IC 443					
PL	11.7 (±0.2) × 10^{-10}	1.76 ± 0.02	—	—	21,651
BPL	11.9 (±0.6) × 10^{-10}	0.57 ± 0.25	$1.95^{+0.02}_{-0.02}$	245^{+16}_{-15}	22,010
W44					
PL	13.0 (±0.4) × 10^{-10}	1.71 ± 0.03	—	—	6,920
BPL	15.8 (±1.0) × 10^{-10}	0.07 ± 0.4	$2.08^{+0.03}_{-0.03}$	253^{+11}_{-11}	7,351

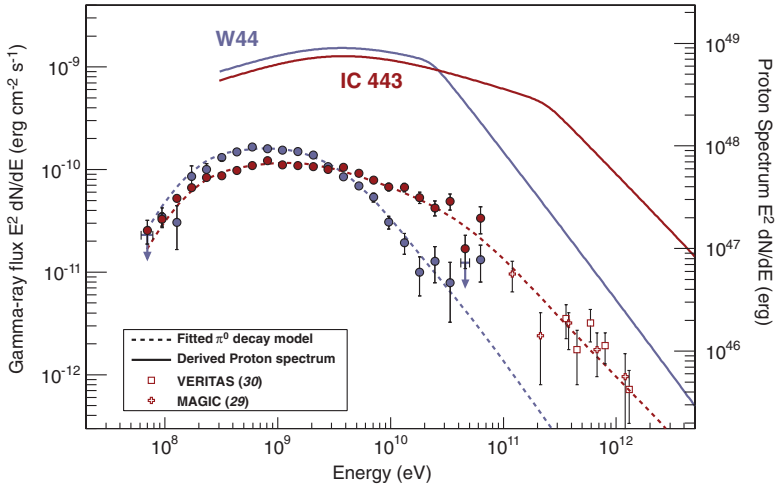

Fig. 3. Proton and gamma-ray spectra determined for IC 443 and W44. Also shown are the broadband spectral flux points derived in this study, along with TeV spectral data points for IC 443 from MAGIC (*29*) and VERITAS (*30*). The curvature evident in the proton distribution at ~2 GeV is a consequence of the display in energy space (rather than momentum space). Gamma-ray spectra from the protons were computed using the energy-dependent cross section parameterized by (*32*). We took into account accelerated nuclei (heavier than protons) as well as nuclei in the target gas by applying an enhancement factor of 1.85 (*33*). Note that models of the gamma-ray production via *pp* interactions have some uncertainty. Relative to the model adopted here, an alternative model of (*6*) predicts ~30% less photon flux near 70 MeV; the two models agree with each other to better than 15% above 200 MeV. The proton spectra assume average gas densities of n = 20 cm^{-3} (IC 443) and n = 100 cm^{-3} (W44) and distances of 1.5 kpc (IC 443) and 2.9 kpc (W44).

References and Notes

1. M. A. Malkov, L. O'C. Drury, *Rep. Prog. Phys.* **64**, 429 (2001).
2. J. S. Warren *et al.*, *Astrophys. J.* **634**, 376 (2005).
3. Y. Uchiyama, F. A. Aharonian, T. Tanaka, T. Takahashi, Y. Maeda, *Nature* **449**, 576 (2007).
4. E. A. Helder *et al.*, *Science* **325**, 719 (2009).
5. G. Morlino, D. Caprioli, *Astron. Astrophys.* **538**, A81 (2012).
6. C. D. Dermer, *Astron. Astrophys.* **157**, 223 (1986).
7. L. O'C. Drury, F. A. Aharonian, H. J. Völk, *Astron. Astrophys.* **287**, 959 (1994).
8. T. Naito, F. Takahara, *J. Phys. G* **20**, 477 (1994).
9. F. W. Stecker, *NASA Spec. Publ. 249* (1971).
10. F. A. Aharonian, L. O'C. Drury, H. J. Völk, *Astron. Astrophys.* **285**, 645 (1994).
11. A. A. Abdo *et al.*, *Astrophys. J.* **706**, L1 (2009).
12. D. J. Thompson, L. Baldini, Y. Uchiyama, http://arxiv.org/abs/1201.0988 (2012).
13. M. Seta *et al.*, *Astrophys. J.* **505**, 286 (1998).
14. P. L. Nolan *et al.*, *Astrophys. J. Suppl. Ser.* **199**, 31 (2012).
15. A. A. Abdo *et al.*, *Science* **327**, 1103 (2010).
16. A. A. Abdo *et al.*, *Astrophys. J.* **712**, 459 (2010).
17. J. Lande *et al.*, *Astrophys. J.* **756**, 5 (2012).
18. M. Ackermann *et al.*, *Astrophys. J. Suppl. Ser.* **203**, 4 (2012).
19. A. Giuliani *et al.*, *Astrophys. J.* **742**, L30 (2011).
20. Y. Uchiyama *et al.*, *Astrophys. J.* **749**, L35 (2012).
21. http://fermi.gsfc.nasa.gov/ssc/
22. The region model fitted to the data includes the SNR of interest (IC 443 or W44), background point sources from the 2FGL catalog (*14*), the galactic diffuse emission (ring_2year_P76_v0.fits), and a corresponding isotropic component (isotrop_2year_P76_source v0.txt).
23. J. R. Mattox *et al.*, *Astrophys. J.* **461**, 396 (1996).
24. See supplementary materials on *Science* Online.
25. Y. Uchiyama, R. D. Blandford, S. Funk, H. Tajima, T. Tanaka, *Astrophys. J.* **723**, L122 (2010).
26. G. Castelletti, G. Dubner, C. Brogan, N. E. Kassim, *Astron. Astrophys.* **471**, 537 (2007).
27. S. Gabici, F. A. Aharonian, S. Casanova, *Mon. Not. R. Astron. Soc.* **396**, 1629 (2009).
28. Y. Ohira, K. Murase, R. Yamazaki, *Mon. Not. R. Astron. Soc.* **410**, 1577 (2011).
29. J. Albert *et al.*, *Astrophys. J.* **664**, L87 (2007).
30. V. A. Acciari *et al.*, *Astrophys. J.* **698**, L133 (2009).
31. M. Tavani *et al.*, *Astrophys. J.* **710**, L151 (2010).

32. T. Kamae, N. Karlsson, T. Mizuno, T. Abe, T. Koi, *Astrophys. J.* **647**, 692 (2006).
33. M. Mori, *Astropart. Phys.* **31**, 341 (2009).

Acknowledgments: The Fermi LAT Collaboration acknowledges support from a number of agencies and institutes for both development and the operation of the LAT as well as scientific data analysis. These include NASA and the U.S. Department of Energy (United States); CEA/Irfu and IN2P3/CNRS (France); ASI and INFN (Italy); MEXT, KEK, and JAXA (Japan); and the K. A. Wallenberg Foundation, the Swedish Research Council, and the National Space Board (Sweden). Additional support from INAF in Italy and CNES in France for science analysis during the operations phase is also gratefully acknowledged. Fermi LAT data are available from the Fermi Science Support Center (http://fermi.gsfc.nasa.gov/ssc).

Supplementary Materials
www.sciencemag.org/cgi/content/full/339/6121/807/DC1
Materials and Methods
Figs. S1 to S3
References (*34*–*39*)

5 October 2012; accepted 12 December 2012
10.1126/science.1231160

Crystalline Inorganic Frameworks with 56-Ring, 64-Ring, and 72-Ring Channels

Hsin-Yau Lin,[1] Chih-Yuan Chin,[1] Hui-Lin Huang,[1] Wen-Yen Huang,[1] Ming-Jhe Sie,[1] Li-Hsun Huang,[1] Yuan-Han Lee,[1] Chia-Her Lin,[2] Kwang-Hwa Lii,[3] Xianhui Bu,[4] Sue-Lein Wang[1]*

The development of zeolite-like structures with extra-large pores (>12-membered rings, 12R) has been sporadic and is currently at 30R. In general, templating via molecules leads to crystalline frameworks, whereas the use of organized assemblies that permit much larger pores produces noncrystalline frameworks. Synthetic methods that generate crystallinity from both discrete templates and organized assemblies represent a viable design strategy for developing crystalline porous inorganic frameworks spanning the micro and meso regimes. We show that by integrating templating mechanisms for both zeolites and mesoporous silica in a single system, the channel size for gallium zincophosphites can be systematically tuned from 24R and 28R to 40R, 48R, 56R, 64R, and 72R. Although the materials have low thermal stability and retain their templating agents, single-activator doping of Mn^{2+} can create white-light photoluminescence.

Crystalline open-framework materials are of interest because of their rich structural chemistry and their use ranging from conventional catalysis, gas separation, and ion exchange to modern high-tech low-*k* materials, zeolite-dye microlasers, high-capacity H_2 and CO_2 gas storage (*1*–*4*), and potential lanthanide-free phosphor materials for light-emitting diodes (*5*–*7*). Their functions are mainly attributed to properties related to pore size. Therefore, pore engineering goals such as enlarging the channels, changing channel shape and connectivity, or modifying the wall composition are critical for creating new materials.

For many years, various zeolite-like structures have been synthesized using both simple and complex preparative techniques. In 1982, the discovery of $AlPO_4$-based zeolite structures (*8*) inspired the synthesis of open-framework metal phosphates. Soon after, the crystal structure of an iron phosphate mineral known as cacoxenite (*9*) was solved, revealing that the structure contained notably large channels with a free diameter of 1.4 nm and openings encircled by 36 polyhedra (36R). These discoveries led to increasing interest in pure tetrahedral and mixed polyhedral frameworks with extra-large channels (table S1). Later, many landmark structures were synthesized

[1]Department of Chemistry, Frontier Research Center on Fundamental and Applied Sciences of Matters, National Tsing Hua University, Hsinchu 30013, Taiwan. [2]Department of Chemistry, Chung-Yuan Christian University, Chungli 320, Taiwan. [3]Department of Chemistry, National Central University, Chungli 320, Taiwan. [4]Department of Chemistry and Biochemistry, California State University, Long Beach, CA 90840, USA.
*To whom correspondence should be addressed. E-mail: slwang@mx.nthu.edu.tw

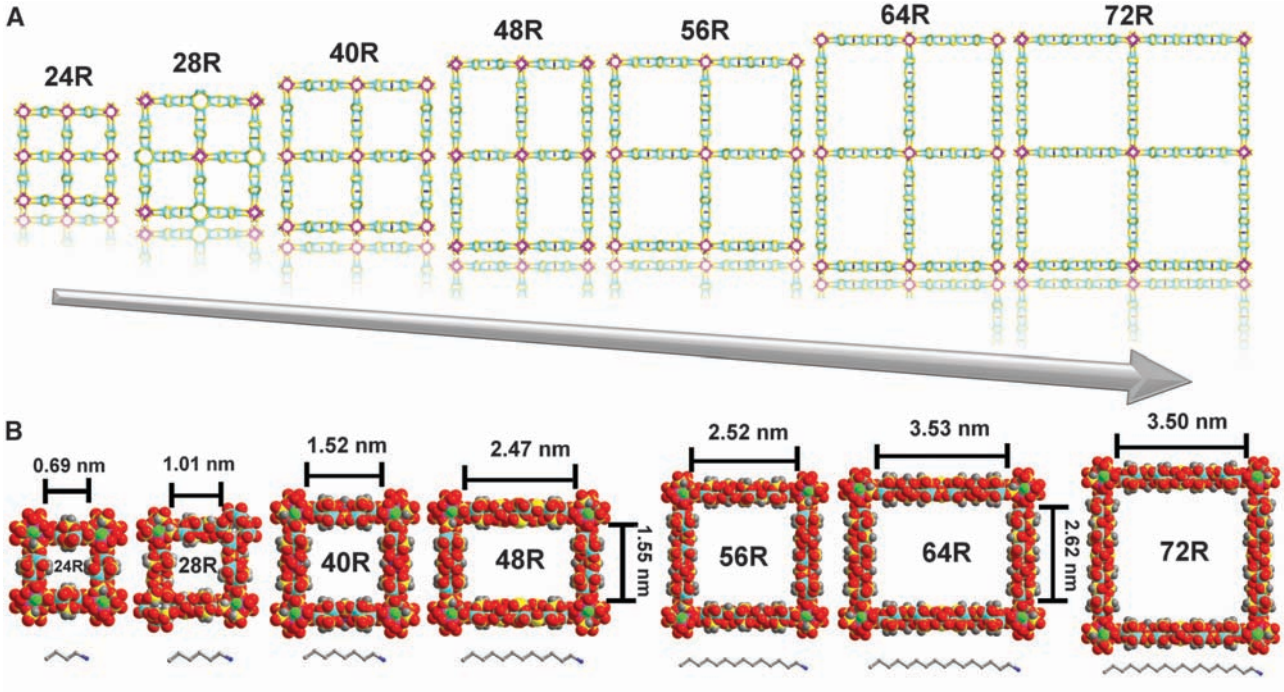

Fig. 1. Systematic expansion of structures with extra-large channels. (**A**) Channel ring size ranging from 24R to 72R. (**B**) Pore diameters spanning the micro and meso regimes. The templates are alkyl monoamines (using a ball-and-stick model) with carbon chain lengths ranging from 4C to 18C.